Self-regulated plasma heat flux mitigation due to liquid Sn vapor shielding

Citation for published version (APA):
van Eden, G. G., Morgan, T. W., Aussems, D. U. B., van den Berg, M. A., Bystrov, K., & van de Sanden, M. C. M. (2016). Self-regulated plasma heat flux mitigation due to liquid Sn vapor shielding. *Physical Review Letters*, *116*(13), 1-5. [135002]. https://doi.org/10.1103/PhysRevLett.116.135002

DOI:
10.1103/PhysRevLett.116.135002

Document status and date:
Published: 01/04/2016

Document Version:
Publisher’s PDF, also known as Version of Record (includes final page, issue and volume numbers)

Please check the document version of this publication:

• A submitted manuscript is the version of the article upon submission and before peer-review. There can be important differences between the submitted version and the official published version of record. People interested in the research are advised to contact the author for the final version of the publication, or visit the DOI to the publisher's website.
• The final author version and the galley proof are versions of the publication after peer review.
• The final published version features the final layout of the paper including the volume, issue and page numbers.

Link to publication

General rights
Copyright and moral rights for the publications made accessible in the public portal are retained by the authors and/or other copyright owners and it is a condition of accessing publications that users recognise and abide by the legal requirements associated with these rights.

- Users may download and print one copy of any publication from the public portal for the purpose of private study or research.
- You may not further distribute the material or use it for any profit-making activity or commercial gain
- You may freely distribute the URL identifying the publication in the public portal.

If the publication is distributed under the terms of Article 25fa of the Dutch Copyright Act, indicated by the “Taverne” license above, please follow below link for the End User Agreement:

www.tue.nl/taverne

Take down policy
If you believe that this document breaches copyright please contact us at:

openaccess@tue.nl

providing details and we will investigate your claim.

Download date: 25. Aug. 2022

Self-Regulated Plasma Heat Flux Mitigation Due to Liquid Sn Vapor Shielding

G. G. van Eden,* T. W. Morgan, D. U. B. Aussems, M. A. van den Berg, K. Bystrov, and M. C. M. van de Sanden
FOM Institute DIFFER-Dutch Institute for Fundamental Energy Research, Partner in the Trilateral Euregio Cluster, De Zaale 20, 5612 AJ Eindhoven, The Netherlands

(Received 1 December 2015; published 1 April 2016)

A steady-state high-flux H or He plasma beam was balanced against the pressure of a Sn vapor cloud for the first time, resulting in a self-regulated heat flux intensity near the liquid surface. A temperature response of the liquid surface characterized by a decoupling from the received heating power and significant cooling of the plasma in the neutral Sn cloud were observed. The plasma heat flux impinging on the target was found to be mitigated, as heat was partially dissipated by volumetric processes in the vapor cloud rather than wholly by surface effects. These results motivate further exploration of liquid metal solutions to the critical challenge of heat and particle flux handling in fusion power plants.

DOI: 10.1103/PhysRevLett.116.135002

Designing an efficacious interface between an intense plasma flux and a solid material has been a challenge for many decades and is among the top issues in realizing fusion energy as a viable energy source on Earth. Plasma-solid interactions under fusion divertor conditions cause continuous material erosion and may result in performance degradation of the plasma-facing components [1–3]. An alternative path is opened by exploiting liquid metals as an interface between the plasma and solid material world [4]; this could potentially alleviate many of the problems of heat exhaust in the divertor. Understanding the unique power-loss channels of liquid metals in contact with a plasma is also highly relevant for other applications, such as metal-arc welding [5].

Additional power handling capabilities such as evaporative cooling [6,7] and the vapor shielding effect [8,9] are inherently available for a liquid surface. The concept of vapor shielding encompasses several physical processes. First, the presence of a neutral cloud in front of the target is foreseen to absorb power by the excitation and ionization of its species. Subsequent radiation occurs isotropically, which reduces the areal power density. Second, the cloud of neutrals leads directly to mass transport losses but also to friction and recombination of impinging plasma particles, ultimately reducing the energy flux to the surface.

In this Letter, for the first time, we provide experimental evidence of steady-state vapor shielding at fusion-divertor-relevant plasma heat (0.5–22 $\mathrm{MW\,m^{-2}}$) and particle fluxes ($>10^{24}\ \mathrm{m^{-2}\,s^{-1}}$). In addition, the experimental validation of using Sn for high-heat-flux applications as previously predicted by modeling [10] is now provided. The work was motivated by the question of the potential of vapor shielding in protecting a surface. To ensure a vapor pressure of similar magnitude as the plasma pressure, the Sn targets were intentionally badly cooled. The power handling characteristics of liquid Sn were compared to those of solid Mo (high heat-handling capability and substrate material for Sn) while being exposed to similar plasma conditions and target cooling in the linear plasma generator Pilot-PSI [11].

The thermal response of the liquid upon receiving an intense plasma heat flux up to 22 $\mathrm{MW\,m^{-2}}$ lasting 5–20 s is described. A self-regulated plasma heat flux mitigation by the liquid-vapor system and a cooling of the electrons in the vapor cloud is observed, leading to a reduction of approximately 30% in the heat flux measured by calorimetry compared to a solid Mo target. Up to 20% of this missing power could be associated with evaporative cooling, whereas $>80\%$ is dissipated via other processes, including radiation from the plasma and cooling and recombination of the plasma due to the vapor cloud.

The linear plasma device Pilot-PSI [11] employs a wall-stabilized thermal arc source [12] to produce a high-flux plasma, which is subsequently confined into a beam by an axial B field (0.4–1.2 T). A power scan of the source resulted in H or He particle (Γ_{part}) and heat fluxes (q) of 0.9–$6.4 \times 10^{24}\ \mathrm{m^{-2}\,s^{-1}}$ and 0.5–22 $\mathrm{MW\,m^{-2}}$, respectively, impinging on the target center. The particle and heat fluxes as functions of the plasma beam radius can be well represented by a 2D Gaussian function (FWHM $\approx$ 10.4 mm). The values were calculated based on the plasma parameters 11 mm in front of the solid Mo target obtained from Thomson scattering (TS) measurements [13]. Heat fluxes were calculated as in [14] assuming $T_i \approx T_e$ (the source produces a thermal plasma), that flow was adiabatic with an isotropic pressure, and that the sheath heat transmission coefficient was set equal to 7.

As TS was not available, the upstream plasma conditions during Sn exposures have been assessed from reference shots on Mo, where we assume that the upstream plasma power should be highly similar for both targets. This is justified because the I-V characteristics of the plasma source were similar for discharges on Mo and Sn targets and no traces of Sn were found in the vicinity of the source after operation. Also, the mean free path of the Sn neutrals

© 2016 American Physical Society

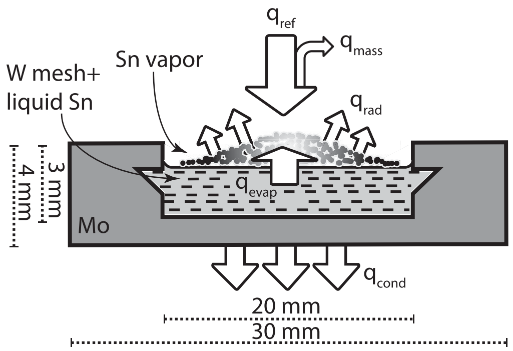

FIG. 1. Cross-section drawing of the Mo capillary-porous-system target filled with Sn. Sn is held in place by a W-mesh structure. The Sn surface receives a plasma heat flux (q_{ref}) which leads to evaporation and subsequent vapor formation in front of the target. The power is dissipated via evaporation and direct mass transport (q_{evap}), radiation by the Sn vapor cloud (q_{rad}), and mass transport resulting from charge exchange (CX) and recombination processes (q_{mass}). The remaining heat is conducted to the cooling water (q_{cond}).

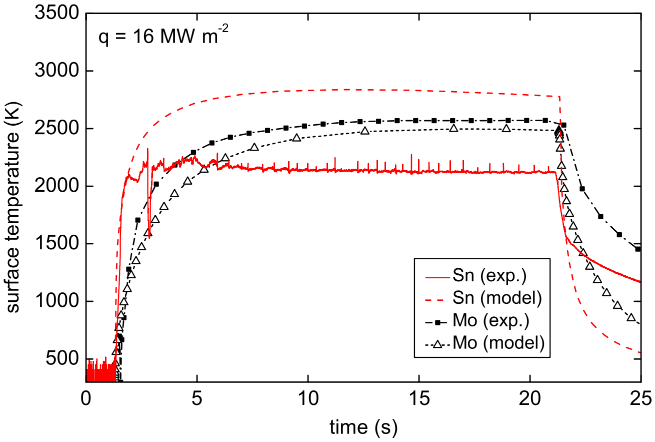

FIG. 2. A comparison of the central surface temperature evolution of liquid Sn and solid Mo during experiment and ANSYS simulations for $q_{\mathrm{ref}} = 16\ \mathrm{MW\,m^{-2}}$. The steady-state temperature of Sn reduces significantly, due to vapor shielding, compared to the conduction-based model without vapor shielding.

(6 mm) is much shorter than the distance to the plasma source (560 mm). The incoming heat flux that must be balanced by heat removal processes in equilibrium conditions is, therefore, the reference heat flux (q_{ref}), which is the measured heat flux received by a Mo target for identical Pilot-PSI operational settings.

A two-channel spectrometer (Avantes ULS2048) was used to measure the radiation intensity in the 299–579 nm range. The detector was focused at the target center (~15° normal to surface) with a spot size of 1 mm. The surface temperature was measured using both an IR camera (FLIR SC7500MB, 4.5 kHz) and a multiwavelength spectropyrometer (FAR Associates FMPI). A temperature-dependent emissivity was applied, previously obtained by comparing the IR and pyrometer data. We assume that any IR emission from the vapor cloud itself is negligible as its density is 8 orders of magnitude lower than that of the liquid. Finally, Sn-neutral emission was recorded by a fast visible camera (Phantom V12, 10 kHz) equipped with a 452.5-nm SnI filter positioned tangentially to the target. The targets consist of a 3-mm-deep Mo cup, where the Sn content is held secured by a stack of W meshes, see Fig. 1. This design is based on the capillary-porous-system principle [15].

The plasma heat flux (q_{ref}) is dissipated via a number of processes. First, power is dissipated by vaporization if evaporated neutrals do not return to the surface (q_{evap}). Second, power is lost by radiation of Sn neutrals and ions in the vapor cloud (q_{rad}) and mass transport (q_{mass}) from the plasma as a result of CX and recombination processes. The remaining heat is transferred to the Mo cup (and, subsequently, cooling water) via conduction and convection of the liquid Sn (q_{cond}). Only low-ionization stages of Sn are reached due to the low temperature in the plasma beam. Ionization to much higher states is expected in a tokamak, which may affect Sn transport and the heat-handling scheme for that geometry.

Figure 2 shows the temperature evolution at the center of the liquid Sn and solid Mo surfaces while exposed to $q_{\mathrm{ref}} = 16\ \mathrm{MW\,m^{-2}}$. Notable differences in thermal response are observed. First, an approximately steady-state surface temperature is reached after ~0.5 s on the liquid surface while the Mo temperature still rises. Second, the temperature ramp in the Sn case does not follow a conduction-based cooling curve, where the temperature increases following Newton's law of cooling until the conducted heat equals the received plasma heating as for the Mo case. Results from 3D finite-element modeling using ANSYS [16] for the same q_{ref} and target materials are shown as well. The mesh has been accounted for in the model for Sn by assuming a 6.25 weight percent of W and applying thermal properties of the mixed material. Only conduction-based cooling has been taken into account, and the absorbed heat by the cooling structure has been modeled to match the experimental results for Mo. Comparing the model with the experimental data for Sn, a reduction of ~700 K compared to expectations at the end of the discharge is observed; this indicates the presence of additional heat dissipation channels for the liquid. It should be noted that the conduction-based model predicts a higher surface temperature for Sn than Mo due to the lower thermal conductivity of the former. The experiment shows, however, a lower final surface temperature for Sn compared to Mo, which gives a clear demonstration that other power-loss processes are important.

Figure 3 shows the central surface temperature at the end of 20 s plasma discharges for both sample types as a function of q_{ref}. It is striking to see that the surface temperature of the liquid Sn is almost independent of the applied heat flux. The final temperature at the solid Mo

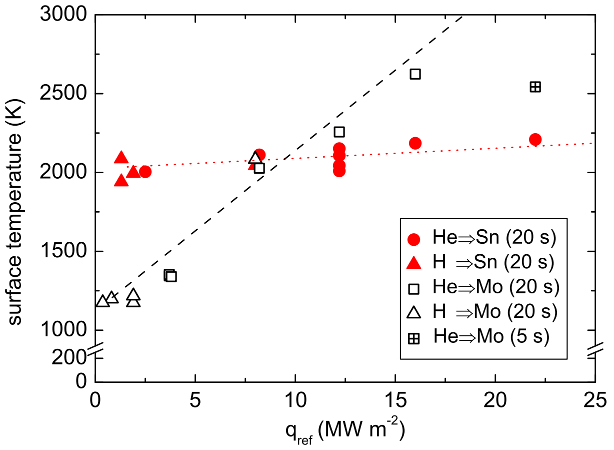

FIG. 3. Temperature of the target surface center after 20 s of plasma exposure for liquid Sn and solid Mo. The lines are drawn to guide the eye. The surface temperature of liquid Sn is almost independent of q_{ref} for the given parameter space. The data point for Mo at 22 $\mathrm{MW\,m^{-2}}$ had a 5 s shot duration to prevent melting the target.

target increases with rising plasma power, as expected. The data point for Mo at 22 $\mathrm{MW\,m^{-2}}$ represents the temperature after a 5 s discharge (to avoid melting the target) and did not reach an equilibrium temperature.

The magnitude of Γ_{part} versus the evaporation flux is assessed now. The vapor pressure (p_v) as function of surface temperature $T(K)$ is calculated as in [17]: $\lg(p_v) = 10.268 - 15332/T$. The flux of particles leaving the surface by evaporation (Γ_{evap}) at a temperature $T(K)$ is assumed to follow from the Langmuir evaporation law [18], $\Gamma_{\mathrm{evap}}(T) = p_v/\sqrt{2\pi m k_B T}$, where k_B represents the Boltzmann constant and m (kg) the mass of Sn. Figure 4 shows Γ_{evap} (calculated using the temperatures as shown in Fig. 3) versus Γ_{part} in the beam center. It is clear from this figure that Γ_{evap} increases linearly in proportion to Γ_{part} for all He discharges and roughly follows $\Gamma_{\mathrm{evap}} = 1.6 \times \Gamma_{\mathrm{part}}$. The Sn evaporation flux during H discharges is seen to remain approximately at the same level. It is proposed that because of the lower mass of H compared to He, the former is affected more strongly by momentum loss via collisions with Sn, therefore resulting in a lower surface temperature and, thus, evaporation rate.

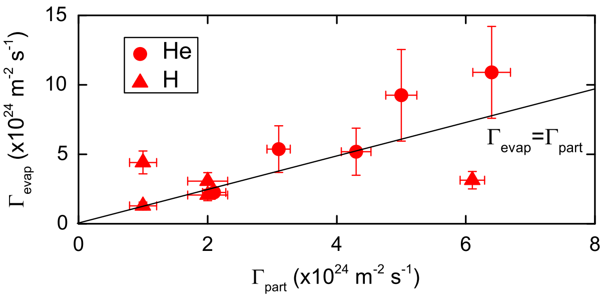

FIG. 4. Evaporation flux (Γ_{evap}) versus the plasma particle flux (Γ_{part}) in the center of the beam for He and H discharges. The solid line represents a perfect equilibrium between plasma and evaporation flux.

The temperature rise of the cooling water was used to determine the average power deposited during each discharge. The average power conducted per unit area, q_{cond}, is $\langle P_{\mathrm{cond}}\rangle/\pi a^2$ where a is the target radius. Results of $\langle P_{\mathrm{cond}}\rangle$ are shown in Fig. 5(a). The nonlinearity of $\langle P_{\mathrm{cond}}\rangle$ at small q_{ref} (and offset) is attributed to a systematic error in the value of the cooling water speed. Further analysis is not affected as ΔP_{cond} is calculated. The total transferred heat is lower for all exposures on Sn compared to exposures on Mo for $q_{\mathrm{ref}} > 2.5\ \mathrm{MW\,m^{-2}}$, and is indistinguishable within or below this. The difference in conducted power between the Mo and Sn targets increases with increasing q_{ref}. The question is therefore by what other dissipation mechanisms this power is removed.

Figure 5(b) shows the difference in conducted power between Sn and Mo at equal q_{ref}, $\langle \Delta P_{\mathrm{cond}}\rangle = \langle P_{\mathrm{cond,Mo}}\rangle - \langle P_{\mathrm{cond,Sn}}\rangle$. As a result of the Gaussian profile of the plasma parameters in the beam, the surface temperature is a circularly symmetric profile and can be well represented by a Gaussian function, $T(r) = T_{\max}\exp(-r^2/2\sigma^2)$. The total power dissipated due to evaporation can now be calculated by multiplying the evaporation flux by the latent heat of vaporization (ΔH_{evap}) and integrating over the target area,

$$\langle P_{\mathrm{evap}}\rangle = (1-Y)\frac{\Delta H_{\mathrm{evap}}}{N_A}\int_0^{2\pi}\int_0^{a}\Gamma_{\mathrm{evap}}[T(r)]\,r\,dr\,d\theta, \quad (1)$$

where N_A represents the Avogadro constant and Y the particle redeposition fraction. The peak surface temperature ($T_{\max}$) during the Sn exposures is presented in Fig. 3. By

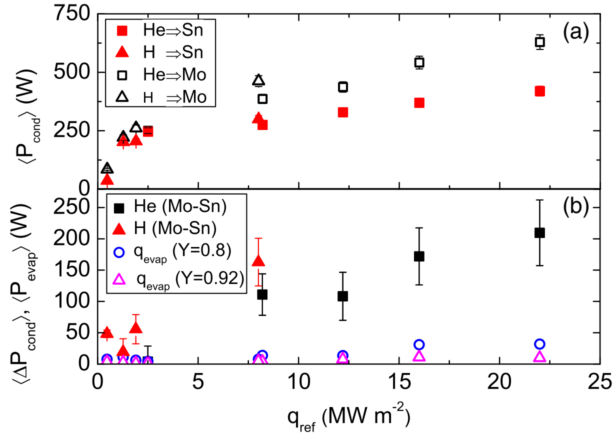

FIG. 5. Power transferred to cooling water as function of q_{ref} for both target types (a) and the difference in conducted power between Mo and Sn (b). The open circles in panel (b) indicate the power dissipated via evaporation assuming $Y = 0.8$. The open triangles represent the lost evaporative power in the case of $Y = 0.92$ [19].

measuring the FWHM of each Gaussian temperature profile, $T(r)$ is obtained and $\langle P_{\text{evap}} \rangle$ is calculated using Eq. (1). Consequently, $q_{\text{evap}} = \langle P_{\text{evap}} \rangle / \pi a^2$.

As the ionization energy of Sn is only 7.34 eV, a large fraction of Sn atoms are ionized and consequently entrained in the plasma and redeposited onto the surface. The removed power for these particles is redeposited onto the surface and is, thus, not a power-loss channel. Redeposition rates of Sn in Pilot-PSI at similar conditions have been previously reported, revealing fractions $Y \geq 0.92$ [19]. In addition, a depletion of Sn in the top layer of mesh in the target was observed after 100 s of plasma exposure, resulting in a loss of 0.45 g Sn. When assuming evaporation without redeposition, 3.4 g is lost for the same duration, yielding a redeposition rate of 87%. The lost power by evaporation for $Y = 0.92$ and $Y = 0.8$ (i.e., 8% and 20% lost particles) are shown in Fig. 5(b). The latter represents a lower bound, accounting for uncertainties in assessing the depletion of Sn in the sample.

The effect of the vapor cloud on the electron temperature (T_e) was studied using spectroscopic analysis. Figure 6 shows a spectrum obtained during a H discharge [20]. The requirement of partial local thermal equilibrium (PLTE) for our H plasma (typically, $n_e = 10^{20}$ m^{-3} and $T_e = 1$ eV) is fulfilled for energy levels $n > 4$ [21]. The density of the upper state (n_j) is proportional to its line intensity (I_j), $n_j \propto (4\pi/A_{ji})I_j$, where A_{ji} represents the Einstein coefficient for this particular transition.

The emission intensities of the following H lines were used: 9-2 (383 nm), 8-2 (388.9 nm), 7-2 (397 nm), 6-2 (410.2 nm), and 5-2 (434 nm) (Balmer series with $n > 4$), followed by a background subtraction. For He discharges, unobscured lines for analysis were selected for each discharge separately from the following set: $1s9s$-$1s2p$ (360 nm), $1s8d$-$1s2p$ (363.5 nm), $1s8s$-$1s2p$ (365.3 nm), $1s7d$-$1s2p$ (370.6 nm), $1s6d$-$1s2p$ (382.1 nm), $1s6s$-$1s2p$ (386.9 nm), $1s4d$-$1s2p$ (447.3 nm).

The ratio of densities of such lines gives T_e, as expressed by the Boltzmann relation [21]

$$\frac{n_j}{n_i} = \frac{g_j}{g_i} e^{-(E_j - E_i)/k_B T_e}. \tag{2}$$

The inset in Fig. 6 shows n_j/g_j versus the upper state energy level (E_j) for a series of high-n H transitions. The PLTE requirement is regarded to be fulfilled when this fit yields a straight line [22]. The inverse slope of the fit then yields T_e [23]. For a given plasma discharge, T_e was determined from averaging multiple spectra during the phase of constant B field in the discharge.

The applicability of this method was verified by cross-checking T_e with values obtained from TS during H exposures on Mo. The methods were seen to yield similar values for T_e, as shown in Fig. 7(a), which gives confidence in the procedure. Values of T_e in the Sn-H and Sn-He near-surface plasma are shown in Fig. 7(b). It is striking to see that T_e in front of the liquid surface is roughly 80% lower than in the case of the solid target, and that it is approximately constant at ∼0.5 eV for $q_{\text{ref}} > 5$ MW m^{-2}. As the region of highest radiation levels lies just above the surface, the emission we observe predominantly comes from there. Therefore, T_e obtained by the Boltzmann method gives the conditions in the Sn-He and Sn-H near-surface plasma.

The reduction in T_e by interaction with the vapor cloud is interpreted to be a two-step process. First, as the ion-neutral cross section is much larger than the electron-neutral cross section due to the mass difference between electrons and ions, it is predominantly the ions that lose their energy by elastic collisions with Sn neutrals. Second, the electrons are

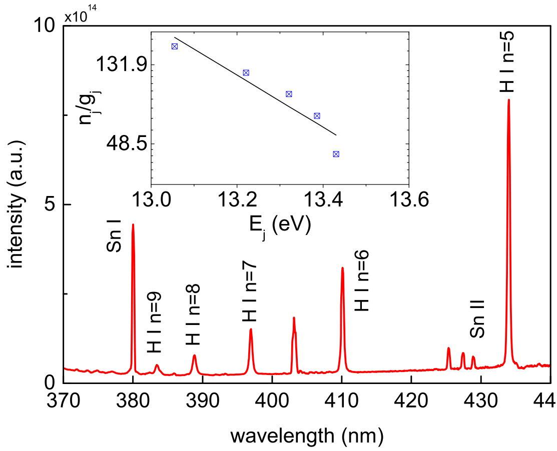

FIG. 6. Typical spectrum showing high-n states of H. The inset gives an example of the Boltzmann method: n_j/g_j is plotted versus the upper state energy level E_j. The inverse slope of the fitted line gives T_e.

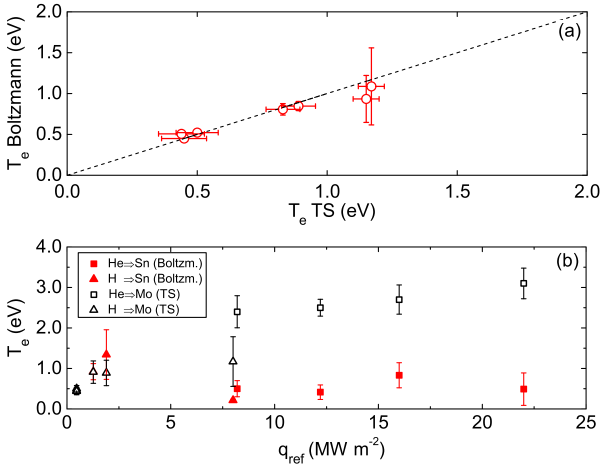

FIG. 7. (a) T_e as a function of q_{ref} for the Boltzmann and TS methods compared for exposures on Mo. (b) Comparison of T_e near a liquid Sn and solid Mo surface for H and He exposures. T_e is found to be significantly lower in front of the liquid surface compared to the solid reference (especially in the case of He).

cooled by an energy exchange with ions, which increases as T_e decreases [24]. The ionization and recombination rates for He at 2 eV and $n_e = 10^{20}\ \mathrm{m}^{-3}$ are almost equal, whereas the recombination rate dominates the ionization rate by a factor of $>10^6$ for $T_e < 1$ eV at this density [25]. Given the measured T_e as shown in Fig. 7(b), the plasma transitions from an ionizing to a recombining regime upon entering the vapor cloud.

It may be noted that Fig. 7(b)shows that the decrease in T_e at a given q_{ref} is larger for H than for He. This observation could be explained by the additional presence of molecular-assisted recombination processes, leading to increased H recombination by a factor of 8–10 at low values of T_e [26]. For both plasma species, we may also consider that CX processes with neutral Sn play a direct role in neutralizing the hot ions, which are then no longer confined by the B field. Overall, these processes are proposed to account for a significant power loss because neutralized particles leave the plasma beam carrying energy away (q_{mass}). This loss channel is in addition to evaporated Sn particles that do not return to the surface (q_{evap}).

In summary, balancing the steady-state plasma pressure with the vapor pressure in front of a liquid surface led to a range of interlinked phenomena, resulting in a reduced target heat flux. Power is dissipated via evaporation (up to 20%), radiation, and mass loss, which reduces the surface heat load by $\sim 1/3$ compared to the solid case. T_e in front of the Sn target is measured to decrease by ~80% compared to the solid reference, indicating that mass transport processes are playing an important or even a dominant role. The overall effect appears self-regulatory, where an increase of heat and particle flux is balanced by an increased evaporation flux leading to an approximately constant heat load received by the liquid plasma-facing component. While the issue of Sn exceeding the tolerable impurity fraction in a magnetic fusion plasma could not be addressed due to differences in magnetic geometry and vapor cloud production, this Letter takes a critical step towards the design of a liquid metal solution for a fusion power plant, namely, the demonstration of the effectiveness of vapor shielding.

The authors wish to thank the Pilot-PSI technical staff and Ronald Wolbeer for the manufacturing of the Sn targets and Egbert Westerhof and Gieljan de Vries for providing valuable input to the manuscript. This work is part of the research program of the Stichting voor Fundamenteel Onderzoek der Materie (FOM), which is financially supported by the Nederlandse Organisatie voor Wetenschappelijk Onderzoek (NWO). It is supported by the European Communities under the contract of association between Euratom and FOM, and was conducted within the framework of the European Fusion Programme.

*g.g.vaneden@differ.nl

[1] A. W. Leonard, A. Herrmann, K. Itami, J. Lingertat, A. Loarte, T. H. Osborne, W. Suttrop (the ITER Divertor Modeling and Database Expert Group, and the ITER Divertor Physics Expert Group), J. Nucl. Mater. **266–269**, 109 (1999).

[2] R. A. Pitts, S. Carpentier, F. Escourbiac *et al.*, J. Nucl. Mater. **438**, S48 (2013).

[3] G. G. van Eden, T. W. Morgan, H. J. van der Meiden, J. Matejicek, T. Chraska, M. Wirtz, and G. De Temmerman, Nucl. Fusion **54**, 123010 (2014).

[4] M. A. Abdou, N. Morley *et al.* (The APEX Team), Fusion Eng. Des. **54**, 181 (2001).

[5] A. Murphy, J. Phys. D **43**, 434001 (2010).

[6] Y. Nagayama, Fusion Eng. Des. **84**, 1380 (2009).

[7] V. A. Evtikhin, A. V. Vertkov, and I. E. Lyublinski, J. Nucl. Mater. **307–311**, 1664 (2002).

[8] T. Sizyuk and A. Hassanein, Nucl. Fusion **54**, 023004 (2014).

[9] J. Gilligan, D. Hahn, and R. Mohanti, J. Nucl. Mater. **162–164**, 957 (1989).

[10] J. W. Coenen, G. De Temmerman, G. Federici, V. Philipps, G. Sergienko, G. Strohmayer, A. Terra, B. Unterberg, T. Wegener, and D. C. M. Van den Bekerom, Phys. Scr. **T159**, 014037 (2014).

[11] G. J. van Rooij, V. P. Veremiyenko, W. J. Goedheer *et al.*, Appl. Phys. Lett. **90**, 121501 (2007).

[12] W. A. J. Vijvers, C. A. J. van Gils, W. J. Goedheer, H. J. van der Meiden, D. C. Schram, V. P. Veremiyenko, J. Westerhout, N. J. Lopes Cardozo, and G. J. van Rooij, Phys. Plasmas **15**, 093507 (2008).

[13] H. J. van der Meiden, R. S. Al, C. J. Barth *et al.*, Rev. Sci. Instrum. **79**, 013505 (2008).

[14] P. C. Stangeby, *The Plasma Boundary of Magnetic Fusion Devices* (Taylor & Francis, London, 2000).

[15] V. A. Evtikhin, I. E. Lyublinski, A. V. Vertkov, V. G. Belan, I. K. Konkashbaev, and L. B. Nikandrov, J. Nucl. Mater. **271–272**, 396 (1999).

[16] ANSYS Multiphysics 15.0 User Manual.

[17] C. B. Alcock, V. P. Itkin, and M. K. Horrigan, Can. Metall. Q. **23**, 309 (1984).

[18] I. Langmuir, Proc. Natl. Acad. Sci. U.S.A. **45**, 452 (1917).

[19] T. W. Morgan, D. C. M. van den Bekerom, and G. De Temmerman, J. Nucl. Mater. **463**, 1256 (2015).

[20] NIST, http://www.nist.gov/pml/data/asd.cfm.

[21] H. Griem, *Principles of Plasma Spectroscopy* (Cambridge University Press, Cambridge, England, 1997).

[22] D. Nishijima, U. Wenzel, K. Ohsumi, N. Ohno, Y. Uesugi, and S. Takamura, Plasma Phys. Controlled Fusion **44**, 597 (2002).

[23] D. U. B. Aussems, D. Nishijima, and C. Brandt, J. Appl. Phys. **116**, 063301 (2014).

[24] N. Ohno, D. Nishijima, S. Takamura *et al.*, Nucl. Fusion **41**, 1055 (2001).

[25] H. P. Summers, Atomic Data and Analysis Structure User Manual, version 2.6, http://www.adas.ac.uk (2004).

[26] A. Y. Pigarov, Phys. Scr. **2002**, 16 (2002).